https://doi.org/10.5194/essd-2025-204
Preprint. Discussion started: 23 June 2025

Data Processing Strategies for Marine Gravity Using Gravity Anomalies and Gravity Disturbances: A Case Study in the Southern Baltic Sea Region.

Krzysztof Pyrchla[1], Gabriel Strykowski[2], Kamil Łapiński[3], Jonathan Kirby[2], Jerzy Pyrchla[3]

[1]Faculty of Electronics, Telecommunications and Informatics, Gdansk University of Technology, Gdansk, Poland
[2] Dept. of Geodesy and Earth Observation, Technical University of Denmark, DTU Space, Lyngby, Denmark,
[3] Faculty of Civil and Environmental Engineering, Gdansk University of Technology, Gdansk, Poland

Corresponding author: Krzysztof Pyrchla (krzysztof.pyrchla@pg.edu.pl)

Abstract

Regional coverage of marine areas by data from marine gravity measurements is important in geodesy and geophysics. However, interpretation of recorded gravity data is still a challenge. This paper addresses the problem of interpreting gravity data using two related, but slightly different methods. The first method involves gravity anomalies, while the second employs gravity disturbances. The main objective of this paper, apart from publishing in some detail the theory behind the two methods, is to demonstrate and briefly discuss the differences in the results. The cause of these different results are mainly interpretation errors in extracting, from marine gravimeter readings, the corrected readings caused by the gravity signal. We show that when both methods are applied to the same data set, which is available at https://doi.org/10.34808/30k6-fj34 (Pyrchla Krzysztof et al., 2025), a model of the marine geoid along the survey lines can be obtained. This can be used either as a direct estimate of the geoid or as an additional constraint by which we can detect and correct the interpretation errors.

Keywords: geodesy; gravity measurement; gravity anomaly; gravity disturbances.

Introduction

Dynamic gravimetric measurements conducted from ships play a crucial role in increasing and densifying the amount of data collected by satellites. Devices currently used for dynamic gravimetric measurements aboard ships are characterized by a measurement uncertainty of 1 mGal or less (Peshekhonov et al., 2022). Terrestrial and marine dynamic measurements, thanks to their high sensitivity and precise localization of the recording site, provide detailed information on gravity distribution. This technology enables the development of regional models of gravity disturbances. An essential component of dynamic gravimetric measurements are Global Navigation Satellite Systems (GNSS). These systems, used for positioning gravimeters, have revolutionized the technology of such measurements (Peshekhonov et al., 2020; Strasser et al., 2019).

Gravimetric data recorded aboard ships in marine areas can be interpreted to determine the spatial distribution of changes in gravity in each region using two methods (Johannes and Smilde, 2009; Kirby, 2003; Sabri et al., 2018). One method utilizes the concept of gravity anomalies, while the other employs the idea of gravity disturbances. Our version of the first method of free-air gravity anomaly modelling was originally developed to process highly uncontrolled automated opportunity marine gravity surveys in Danish waters with patchy and incomplete data. The marine gravimeter for these surveys was piggybacked on scheduled hydrographic surveys. Although high

https://doi.org/10.5194/essd-2025-204
Preprint. Discussion started: 23 June 2025

quality, but sometimes patchy, 2D RTK navigation (latitude, longitude) was available for these automated surveys, detailed information about the sensor height above the ellipsoid was simply not available. The data processing method presented here works also for controlled marine gravity surveys for which more complete survey information is available. In the paper we explain why a pier level in the reference harbor should be used as the vertical level for the gravity anomaly method. The second method of gravity disturbance modelling makes full use of 3D GNSS navigation of the gravity sensor at sea and a careful referencing of the marine gravimeter readings and reference gravity to the sensor height in harbors. Our version of the two methods translates the marine gravimeter readings directly to pseudo gravity anomalies and pseudo gravity disturbances at sea; i.e. the noisy estimates of the two modelled quantities. Another option is to model from marine gravimeter readings the absolute gravity at sea and, subsequently, to subtract the normal gravity. After applying recommended standard corrections in the manual on the factory filtered marine gravimeter readings (such as the linear drift and Eötvos corrections) the data processing in the two methods differs slightly because the gravity disturbance method includes also ellipsoidal heights from 3D GNSS processing which add noise. Nevertheless, the data processing in both methods is roughly similar, and the goal of both methods is to separate the gravity signal and noise along the survey lines. Surprisingly, and as we show here, having both data types (free-air gravity anomalies? and gravity disturbances) yields geoid/quasi-geoid heights along the survey lines. In the context of marine gravimetry, at this stage of consideration, interpretations using both methods are assumed to produce useful results. In this study, we use both methods for interpreting gravimetric data to compare the obtained results.

In 2021 and 2023, a research team from Gdańsk University of Technology conducted two gravimetric measurement campaigns in the southern Baltic Sea. During the preparation phase, the team reviewed descriptions of campaigns conducted by other teams that had performed marine gravimetric surveys (Förste et al., 2020; Ince et al., 2020; Lu et al., 2019). Data registered during the campaign are available in the repository at https://doi.org/10.34808/30k6-fj34. The data description is given in the section “data availability.”

During marine gravimetric measurements, the gravimeter sensor registers additional accelerations not related to gravity. For example, sea waves cause constant, unpredictable motion in all measurement sensors. To accurately capture vessel movements, additional GNSS receiver was installed aboard the ship. This device provided data to determine corrections for vertical accelerations caused by the ship's motion and the dynamic effect resulting from the cross-coupling of horizontal and vertical acceleration components.

During the campaigns, all necessary data for interpreting the recorded gravity signals were collected. The distribution of measurement profiles is shown in Figure 1, which also indicates the locations of Ground-Based Augmentation System (GBAS) stations in the GNSS measurement area.

https://doi.org/10.5194/essd-2025-204
Preprint. Discussion started: 23 June 2025

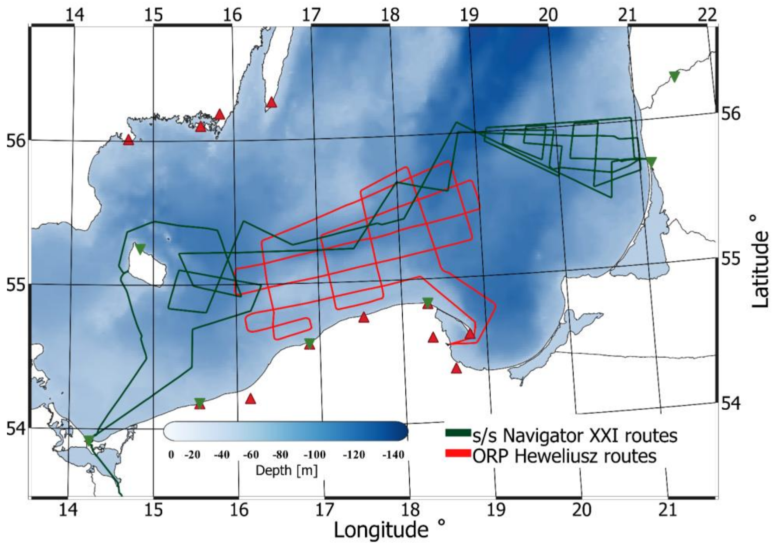

Fig. 1: Marine gravimetric campaign with measurement profiles marked and showing the locations of the 16 reference stations: blue for HxGN Smartnet and red for SWEPOS. The blue shading shows ocean depth.

The verification procedure for the obtained regional gravity grids involved comparing results obtained by both methods. The goal of this study is to evaluate spatial differences between the results of these methods. This is achieved by applying different approaches to marine gravimetric data processing to obtain reliable stochastic realizations of gravity disturbances and anomalies in the target area. This approach enables the quantification of uncertainties in gravity disturbances and anomalies.

This paper is organized as follows. The description of the collected data and details of the methodology used for the measurement campaigns are presented in Section 2 and Appendix A, which describes signal frequency recording and noise spectra during the voyage. Post-processing using both methods and the results in the form of gravity disturbance maps are presented, discussed, and analyzed in Section 3. The summary and conclusions can be found in Section 4.

2. MATERIALS AND METHODS

2.1 Preparation and Recording of Gravimetric Data

During the preparatory stage, a reference point was established on the quay. Gravimetric measurements recorded during the marine campaign were linked to Polish gravimetric control points, resulting in the creation of a new point (No. 407). The gravimetric value was transferred from the nearest absolute first-order points: the permanent gravimetric point 5403 (POLREF-GORA DONAS) and point 363 (GDAŃSK ABS) (ID 5418234342.000). The values for these points were obtained from the National Register of Fundamental Geodetic, Gravimetric, and Magnetic Networks (PRPOG), managed by the Polish Head Office of Geodesy and Cartography.

https://doi.org/10.5194/essd-2025-204
Preprint. Discussion started: 23 June 2025

Open Access Earth System Science Data Discussions

Two relative gravimeters, both Scintrex CG5 (Fig. 2a and 2b), were used to transfer the gravity values. The next stage of preparation involved installing the MGS-6 gravity system (Fig. 2d) and GNSS receivers (Fig. 2c) on the ship.

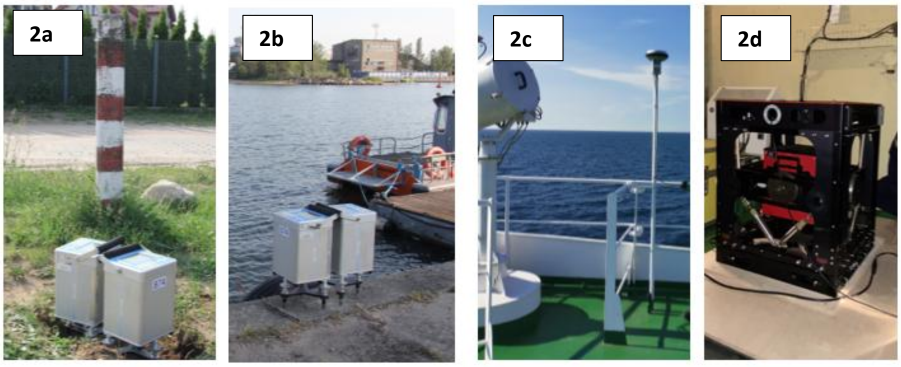

Fig. 2: Gravimetric measurements at the control point and in the port (Figs 2a,b), along with the installation of the Marine Gravity System MGS-6 (Fig. 2d) and GNSS antenna (Fig. 2c) on the ship.

After installing the measurement devices, the offset of these devices and the balance of the lever arm (gravimeter, IMU, antennas, GNSS, and reference point on the ship's side) were measured with an accuracy of less than 0.01 m using a total station. The primary challenge was the vertical tilting of the ship; although imperceptible to humans, it was clearly noticeable during measurements.

The gravity value of the new point, No. 407, at the quay (g_{407} = 981,445.718 mGal) was taken as the reference for gravity data on the ship and is based on the height difference between point No. 407 and the sensor of the MGS-6 Micro-g LaCoste gravity system (dh = 0.751 m). The gravity gradient in air (0.3086 mGal/m) was applied. The transfer of the gravity value was conducted one hour before departure and one hour after arrival at the port. During measurements, the entire crew remained onboard. The measurements determined the height difference between the ship's coordinates frame offset point on the side and the reference point on the quay, using a surveyor's level.

The next stage involved preparing measurement campaign plans and continuously recording gravimetric signals, echo sounder data, and GNSS data throughout the campaigns. The campaign plan included the arrangement of measurement profiles along the route to ensure each profile recorded useful signals. The distance between profiles exceeded four nautical miles. Because after changing course, the stabilization of heading requires some time, the data recorded up to five minutes after each turn where excluded form processing. This allowed sufficient time for the gravimetric sensor to stabilize after each maneuver. The layout of measurement profiles included course intersections at angles greater than 60 degrees.

Plans for campaign routes were prepared a priori to the vessel left the harbor however, some room for future adjustments was left. These adjustments where during campaign made to mitigate the effect of changes in weather conditions, wind speed and direction, and wave height and direction. During gravimetric measurements onboard

https://doi.org/10.5194/essd-2025-204
Preprint. Discussion started: 23 June 2025

ships, the gravity meter measures a combination of the gravity field and any inertial accelerations due to the ship's motion. That is, gravitational and inertial forces are physically combined and projected onto the sensitive axis of the gravimeter. Hence, adjustments to the plans aimed to minimize the influence of inertial accelerations on the gravity measurement.

The MGS-6 next-generation marine gravity system measures signals with an accuracy of 10^{-8} m/s². However, during useful signal measurements, it records all other accelerations with the same sensitivity. This results in noise levels in the recorded signal being hundreds of times greater than the gravity signal (Dehlinger, 1978; Panet et al., 2011). The accuracy of the gravimeter measurement is also influenced by the Eötvös effect, Harrison effect, and cross-coupling. Therefore, a critical task in this case was to develop a measurement technology to eliminate the maximum number of sources of interference. This technology is directly linked to interpreting the signals recorded on the ship during the measurement campaign. Since the evaluation of recorded gravimetric signals without prior processing is complex, efforts were made to reduce acceleration noise to an acceptable level—a goal inherent in all dynamic gravimetric measurements conducted onboard ships (Forsbergbi et al., 2012; Guo et al., 2014).

According to the device data sheet provided by the manufacturer, it is assumed that the Micro-g LaCoste gravity system has a measurement accuracy of 1 mGal (Przyborski et al., 2019) for ships over 40 m in length. However, after applying all necessary dynamic corrections derived from signals recorded by additional measurement sensors, the extracted gravimetric signal from the recorded data achieves an uncertainty better than the manufacturer's specifications.

2.2 GNSS Data Preparation and Recording.

GNSS data play a crucial role in obtaining useful signals in gravimetric measurements, specifically for horizontal and vertical positioning. To collect a large amount of GNSS data, the ships were equipped with the following additional receivers: 4x Leica GS18 with CS20 controllers, and 2x Leica GR30 receivers with AR10 antennas.

To properly process raw GNSS data, the data were obtained from reference stations of the HxGN Smartnet network (Koivula et al., 2018) located along the Polish coastline. For better post-processing geometry, data were also acquired from Swedish reference stations of the SWEPOS system (Fors et al., 2021; Jonsson et al., 2003; Lidberg et al., 2016) located along Sweden's southern coast, as well as Danish stations in Tejn (station code: TEJH00DNK) and Lithuanian stations in Klaipeda (station code: KLAI) and Skuodas (station code: SKDA). Precise GPS and GLONASS satellite ephemerides were included in the computational process using data from the International GNSS Service (IGS) (Tran et al., 2020).

Considering the distance between the coasts of Poland, Sweden, Denmark, and Lithuania, the voyage duration, and the ship's route on the Baltic Sea, it was decided to prepare GNSS data in the office during post-processing (Strasser et al., 2019). Software such as Leica Infinity (Belloni et al., 2022; Di Rita and Hanson, 2022) and algorithms developed by the research team (Stepanov et al., 2020) were used. Post-processing included verifying GNSS data, campaigns, and the compatibility of rover types and reference stations to avoid inconsistencies.

The following post-processing parameters were applied:

https://doi.org/10.5194/essd-2025-204
Preprint. Discussion started: 23 June 2025

1. To limit the effect of ship roll and pitch in heavy seas, the antenna elevation mask was set to 25 degrees. This excluded those satellites close to the horizon, which could otherwise appear and disappear from the antenna's line of sight, focusing on those higher above the horizon for uninterrupted contact (Kim and Park, 2017).
2. Precise ephemerides for GPS and GLONASS signals.
3. Extended uncertainty resolution to 300 km, ensuring GNSS observations at sea were computed based on coastal GBAS systems (Kalaycı et al., 2016).
4. Maximum baseline length of 300 km, aligning with uncertainty resolution for coastal GBAS-based computations.
5. Minimum observation time for typical observations: 300 seconds, eliminating short-term observations caused by antenna oscillations.

These parameters yielded 187,250 baselines and calculated points. Since the measurement antenna was installed on a continuously moving ship, one-second observations were recorded, ensuring no redundant reference stations along the ship's route, demonstrating the importance of accurate horizontal and vertical positioning during marine gravimetric measurements.

2.3 Interpretation of Recorded Data in Measurement Campaigns.

In physical geodesy, and using notation from [24], we conceptually deal with real gravity field where the field point is called P and a (model) normal gravity field where the field point is called Q. Gravity measurements at sea are associated with a specific point in space and time (e.g. the sensor point of marine gravimeter) which throughout this paper is called P, $P = P(\varphi_P, \lambda_P, h_P)$ and where φ_P is the geodetic latitude, λ_P is the geodetic longitude and h_P the ellipsoidal height of P. A normal gravity vector at the sensor point, i.e. for $Q = P$, is denoted $\boldsymbol{\gamma}_{Q=P}$ and a gravity vector is denoted $\mathbf{g}_P$. Neglecting the small angle between the ellipsoidal normal through P and the true direction of the gravity vector (the deflection of the vertical [24]) we approximate the vertical component of the two vectors along the ellipsoidal normal through P with scalar quantities, the absolute gravity $g_P = |\mathbf{g}_P|$ and the normal gravity $\gamma_{Q=P} = |\boldsymbol{\gamma}_{Q=P}|$. We use notation P_0 to denote a point on the geoid along the ellipsoidal normal through P. Furthermore, Q_0 denotes a point on the ellipsoid on the same ellipsoidal normal through P, see **Fig. 3**. For P_0 the ellipsoidal height h_{P_0} is simply the geoid height N_P, $h_{P_0} = N_P$. Not shown on **Fig. 3** is the virtual point P^* which we introduce in Appendix A in connection with the gravity anomaly method, and which is a point on the ellipsoidal normal through P which is at the same orthometric height H above the geoid as the pier point in the reference harbor, i.e. $H_{P^*} = H_{pier}$.

https://doi.org/10.5194/essd-2025-204
Preprint. Discussion started: 23 June 2025

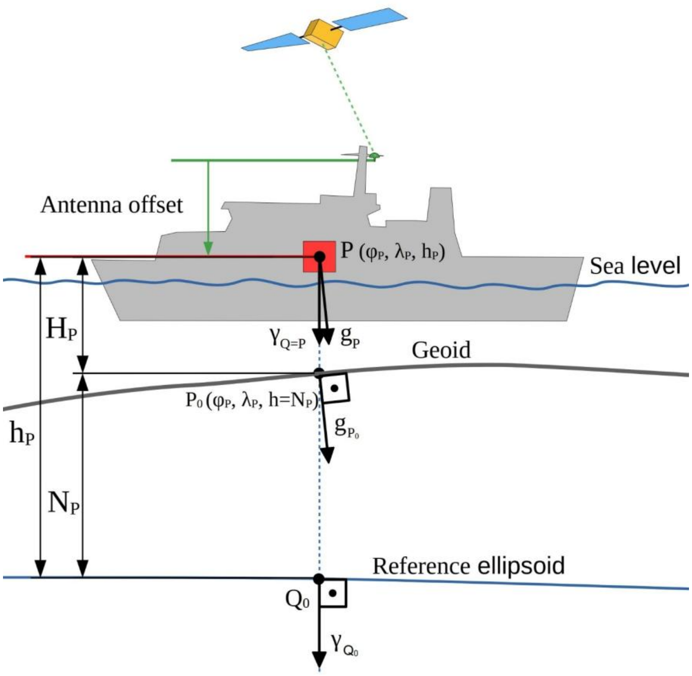

Figure 3: *Marine gravimetric measurements are associated with a sensor point P which moves with the vessel in time and space along the survey lines. Referring to the detailed explanation in the text above: $\gamma_{Q=P}$ is the normal gravity and g_P is the absolute gravity. The virtual point P^* discussed in connection with the gravity anomaly method (see below and Appendix A.3) is not shown on the figure to keep it simple but explained in some detail in the paper. P^* lies on the ellipsoidal normal perpendicular to the reference ellipsoid surface at point Q_0 which is depicted on the figure as the dashed line passing through Q_0, P_0, and P.*

In Appendix A we provide some more details and comments on the processing methods that we use. Both methods make use of the fundamental equation of relative gravimetry:

$$g_P = g_{ref} + \alpha \left[\tilde{r}_P - r_{ref} \right] \tag{1.1}$$

where g_P is the absolute gravity of a marine gravimeter sensor point P along the survey line, g_{ref} is the reference absolute gravity value on the harbor (which for the gravity disturbance method is the sensor height in the reference harbor), α is the scale factor of the marine gravimeter, r_{ref} is the (gravity reading in the reference harbor, and $\tilde{r}_P$ is the corrected marine gravimeter reading for the sensor point P on the ship. We provide some more comments in Appendix A.1

In Appendix A.2 we discuss a 3D processing method of gravity disturbances. From 3D GNSS navigation data we obtain the ellipsoidal height of the antenna from which, via the antenna offset, we get h_P the ellipsoidal height of the sensor. From this we can model the gravity disturbance δg_P

https://doi.org/10.5194/essd-2025-204
Preprint. Discussion started: 23 June 2025

$$\delta g_P = g_P - \gamma_{Q=P} \tag{1.2}$$

In order to obtain $\gamma_{Q=P}$ we compute γ_{Q_0} on the GRS80 ellipsoid (see Fig. 3.) and use a standard constant free-air normal gravity gradient $\frac{\partial \gamma}{\partial h} = -0.3086$ mGal/m yielding

$$\gamma_{Q=P} = \gamma_{Q_0} + \frac{\partial \gamma}{\partial h} h_P \tag{1.3}$$

The final formula Eq. (A.2.4), which is derived and explained in some detail in Appendix A.2, directly computes gravity disturbances values at sea, δg_P, from the corrected marine gravimeter readings, $\tilde{r}_P$, using detailed modelling of the gravity disturbance δg_{ref}, where $g_{ref} = g_{sensor}$ in the reference harbor:

$$\delta g_P = \left[\delta g_{ref} + \alpha\left(\tilde{r}_P - r_{ref}\right)\right] - \left(\left[\gamma_{Q_0} - \gamma_{Q_{0,ref}}\right] + \frac{\partial \gamma}{\partial h}\left[h_P - h_{P_{ref}}\right]\right) \tag{1.4}$$

For the 2D gravity anomaly method, which is derived and explained in some detail in Appendix A.3, we assume that the pier point associated with the harbor tie measured in the reference harbor with land gravimeters, P_{pier}, is the reference point P_{ref} associated with the reference absolute gravity value g_{ref}, $g_{ref} = g_{pier}$ in Eq. (1.1). With this definition, there seems to be an apparent mismatch between g_{ref} and r_{ref} in the reference harbor in a sense that these values refer to two different points in space, and are thus affected differently by the gravitational attraction of the pier. In Appendix A.3 we argue that this mismatch corresponds to the bias of the results. However, the careful matching between g_{ref} and r_{ref} in the reference harbor gets often lost at sea because certain corrections for the sea state, the wind and the weather, for example, cannot be done accurately enough so that the matching between g_P and $\tilde{r}_P$ while at sea is maintained.

Keeping the definition of g_{ref} as described above gives the advantage of geodetic control from land. The pier point can be visited with a portable RTK antenna so that the orthometric height of the pier point in the national height system H_{pier} and the ellipsoidal height h_{pier} can be measured to high accuracy (given a geoid model). From this we can determine the free-air gravity anomaly at the pier point Δg_{pier}:

$$\Delta g_{pier} = g_{pier} - \left[\gamma_{0,pier} + \frac{\partial \gamma}{\partial h} H_{pier}\right] \tag{1.5}$$

where $\gamma_{0,pier}$ is the normal gravity on the ellipsoid at the pier point.

Let us define a virtual point at sea P^* with the same orthometric height H_{P^*} as the pier point in the reference harbor, i.e. $H_{P^*} = H_{pier}$. We can compute the free-air gravity anomaly for such a virtual point at sea using

$$\Delta g_{P^*} = g_{P^*} - \left[\gamma_{0,P^*} + \frac{\partial \gamma}{\partial h} H_{P^*} \right] \tag{1.6}$$

Using Eq. (1.1) for the virtual point, i.e. $P = P^*$, we get

$$g_{P^*} = g_{pier} + \alpha \left[\tilde{r}_{P^*} - r_{ref} \right] \tag{1.7}$$

As explained in Appendix A.3, using $H_{P^*} = H_{pier}$ and setting $h_{P^*} = H_{P^*}$ we arrive at

$$\Delta g_{P^*} = \Delta g_{pier} + \alpha \left[\tilde{r}_{P^*} - r_{ref} \right] + \left[\gamma_{0,pier} - \gamma_{0,P^*} \right] \tag{1.8}$$

The advantage of the above equation is that the free-air gravity anomalies are only weakly dependent on height. This is explained in Appendix A.3. The final expression for the marine gravity sensor point P, where the orthometric height of this point H_P is unknown for this method we get after some derivations:

$$\Delta g_P \approx \Delta g_{P^*} \tag{1.9}$$

Finally, and as explained in Appendix A.4, using Helmert's projection $h_P = H_P + N_P$ for the sensor point P, and using Eq. (1.6), but for gravity disturbances

$$\delta g_P = g_P - \left[\gamma_{Q_0} + \frac{\partial \gamma}{\partial h} h_P \right] = g_P - \left[\gamma_{Q_0} + \frac{\partial \gamma}{\partial h} \left(H_P + N_P \right) \right] \tag{1.10}$$

we finally obtain

$$\delta g_P = \Delta g_P - \frac{\partial \gamma}{\partial h} N_P \tag{1.11}$$

Which is consistent with the theory presented in (Kirby, 2003)

A simple rearrangement of Eq. (1.11) yields

$$N_P = \left(\Delta g_P - \delta g_P \right) / \left(\partial \gamma / \partial h \right) \tag{1.12}$$

https://doi.org/10.5194/essd-2025-204
Preprint. Discussion started: 23 June 2025

Open Access Earth System Science Data Discussions

In summary, equation (1.4) defines the gravity disturbance method, while equation (1.8) defines the gravity anomaly method. Fig. 3 illustrates the concepts at sea.

The data processing starts for both methods with the factory filtered 1 Hz gravity readings in the internal counter units of the marine gravimeter. These readings are then corrected using standard corrections described in the instrument's manual (linear drift based on harbor ties, Eötvos correction and, possibly, the cross-coupling correction). The result is the corrected reading, $\tilde{r}_P$, that appears in the fundamental equation of relative gravimetry, Eq. (1.1), and also in Eqs (1.4) and (1.8) for the two methods. We prefer not to filter $\tilde{r}_P$ additionally prior to the interpretation. Thus, the two quantities that we construct through Eqs (1.4) and (1.8) are noisy due to the noise in $\tilde{r}_P$ that we purposely do not remove. In Eq. (1.4) there is also an additional measured data input, the ellipsoidal height h_P, which is obtained from processing 3D GNSS data along the ship's route. This adds noise to the transformed quantities, in addition to noise caused by $\tilde{r}_P$ common to both methods. We call such noisy transformations of the measured data "pseudo", i.e. pseudo gravity disturbances and pseudo free-air gravity anomalies.

The (standard) corrected readings, $\tilde{r}_P$, and the modelled ellipsoidal heights, h_P, from 3D GNSS data processing may both contain undiscovered systematic errors. The constructed noisy quantities can be used to detect and to diagnose these disturbing effects. For example, a standard analysis of the processing results at crossover points between survey lines is a measure of such uncorrected systematic errors in the measured and transformed data. In this context, and without further details, both transformed quantities are robust with respect to stationarity of the true values at crossover points. Because of the time-varying sea level, the sensor height for the same horizontal location (latitude, longitude) may not necessarily be the same at different times associated with crossing survey lines. However, and for the same formal reasons that led to the approximation in Eq. (1.9), the true free-air gravity anomaly for a given location of the crossover point only weakly depends on height. Without further explanation, and as a consequence of Eq. (1.9), if the free-air gravity anomalies Δg_P depend only weakly on height, this is also true for gravity disturbances δg_P.

Summarizing the above, the first method described (the gravity anomaly method) extracts information about gravity anomalies from recorded gravimetric data during post-processing. This method does not depend on detailed GNSS height data recorded during the campaign. The second method, which uses precise height data, is the gravity disturbance method. This approach requires more effort during the data collection and interpretation phases to determine the height distribution along measurement profiles.

The measurement campaigns mentioned in this paper were conducted with the highest possible precision to record the horizontal and vertical positions of the measurement points. These efforts, along with the significant amount of accurately recorded gravimetric signals, enabled the post-processing of the dataset using both the gravity anomaly and gravity disturbance models.

3. RESULTS

https://doi.org/10.5194/essd-2025-204
Preprint. Discussion started: 23 June 2025

Data processing from noisy pseudo free-air gravity anomalies and pseudo gravity disturbances with the aim of extracting the gravity model along survey lines is, to some extent, a subjective interpretation. On the one hand the actual readings of the marine gravimeter are included in the interpretation through pseudo anomalies of both types. On the other hand the stationarity of the gravity field quantities at cross points may require that the gravity model deviates from the gravimeter reading. There is a delicate balance between the two and the additional corrections of the (already corrected) gravimeter readings, $\tilde{r}_P$, or even additional corrections of the systematic errors in ellipsoidal heights, h_P, should be based on solid information. Good statistics at crossover points are a consequence of adequate corrections and are not the goal of processing. Which information to use to improve the correction budget is outside the scope of this paper except in one case: the geoidal heights derived through Eq. (1.12).

The results that we present follow pseudo free-air gravity anomalies and pseudo gravity disturbances. The first analysis was conducted using the gravity anomaly method on the signals recorded aboard ORP "Heweliusz" and s/s "Nawigator XXI" (Pyrchla Krzysztof et al., 2025). The spatial distribution of gravity anomalies along the ORP "Heweliusz" measurement profiles is presented in **Figure 4**. The corresponding spatial distribution of gravity disturbances along the measurement profiles is presented in **Figure 5**.

In the eastern part of the measurement profiles, the gravity anomaly values show a minimum corresponding to the Gotland Deep area. In the western profiles, there is a peak in gravity anomaly values (at approximate latitude 55.2°N, longitude 16°E) that correlates with the shallow depths in this part of the Baltic Sea.

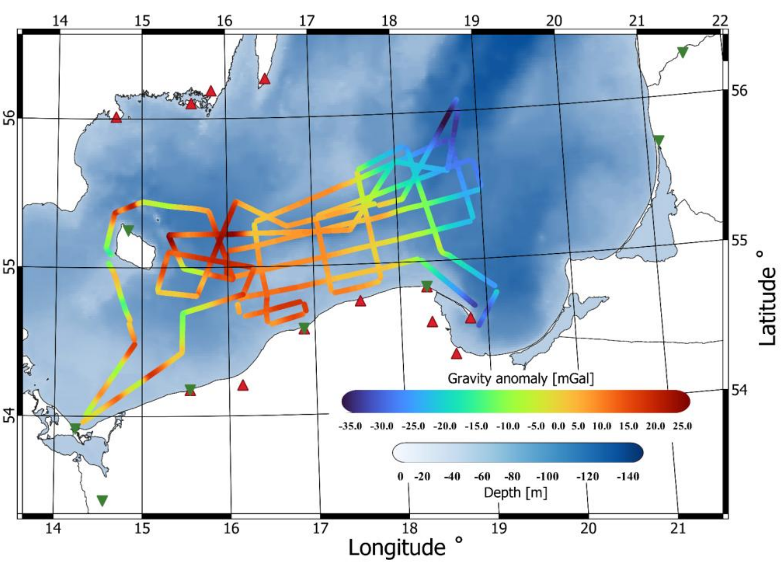

Figure 4: Spatial distribution of gravity anomalies along the measurement profiles.

https://doi.org/10.5194/essd-2025-204
Preprint. Discussion started: 23 June 2025

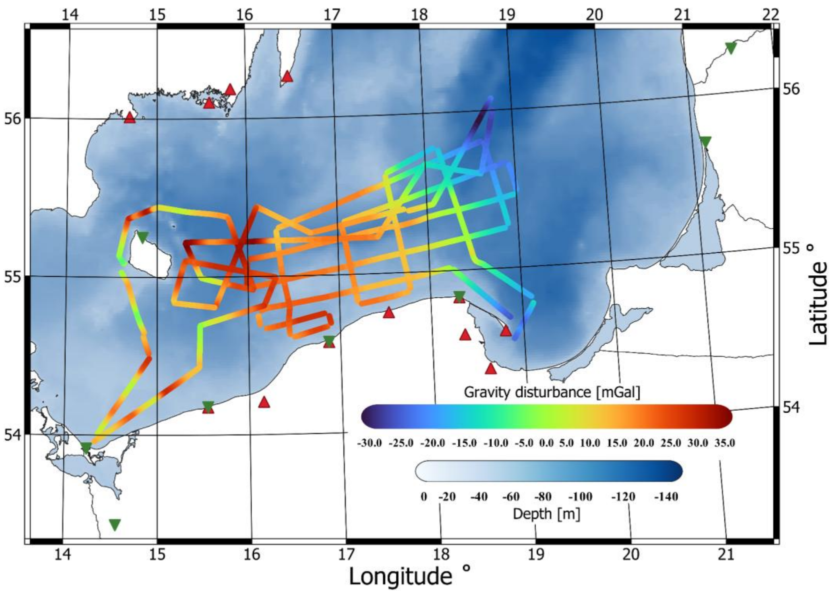

Figure 5: Spatial distribution of gravity disturbances along the measurement profiles.

Table 1 and Table 2 show, respectively, the statistics at crossover points for gravity disturbances and free-air gravity anomalies. The number of crossover points is not that great (18 for ORP Heweliusz survey, 9 for Nawigator XXI survey and 18 cross-survey), but the crossing statistics indicate that the results are of acceptable quality and that there are no significant differences in the results from the two methods.

Table 1: The statistics of crossing points values for ORP Heweliusz and s/s NawigatorXXI campaign. Values obtained for 2D processing using free air anomalies.

	ORP Heweliusz	s/s Nawigator XXI	between campaigns
mean [mGal]	0.131	0.120	0.765
std [mGal]	0.494	0.670	1.187
max [mGal]	1.426	1.096	2.329
min [mGal]	-1.222	-1.398	-1.663
N	18	9	18

Table 2: The statistics of crossing points values for ORP Heweliusz and s/s NawigatorXXI campaign. Values obtained for 3D processing using gravity disturbances.

	ORP Heweliusz	s/s Nawigator XXI	between campaigns
mean [mGal]	0.251	0.186	0.72

https://doi.org/10.5194/essd-2025-204
Preprint. Discussion started: 23 June 2025

std [mGal]	0.543	0.687	1.162
max [mGal]	2.183	1.108	2.119
min [mGal]	-1.535	-1.181	-0.573
N	18	9	18

Further analyses focused on the differences between gravity disturbances and free-air anomalies along individual profiles. The visualization of these differences on the profiles conducted by ORP "Heweliusz" is presented in **Figure 6**.

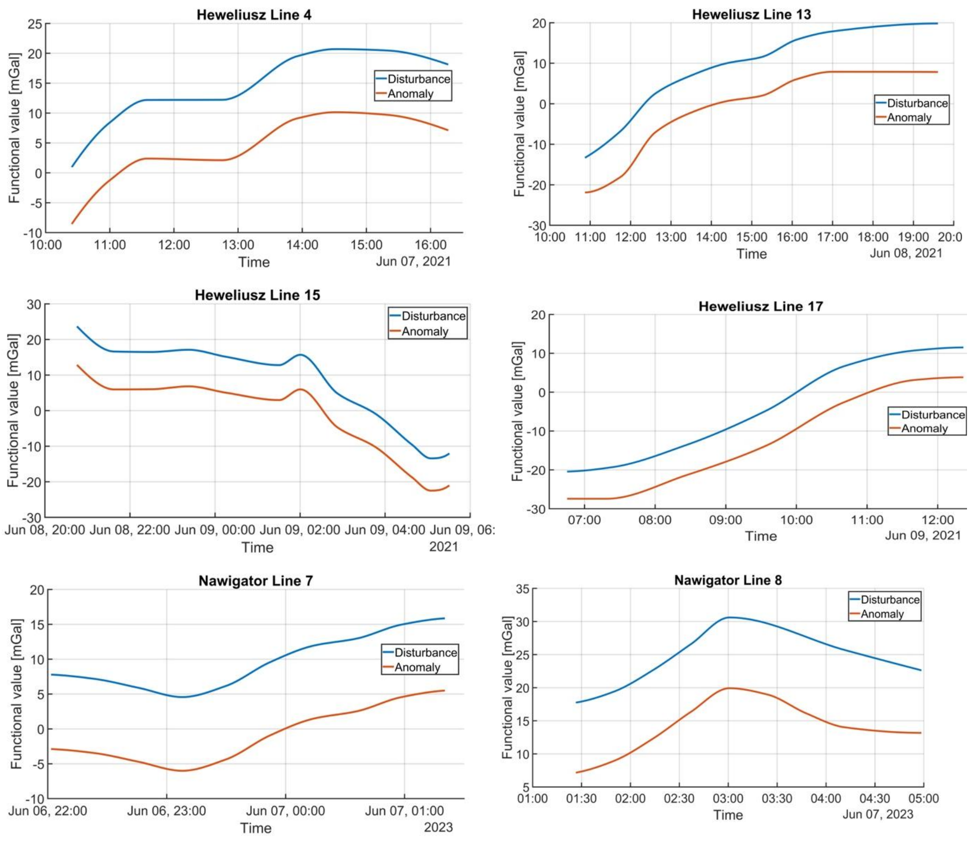

https://doi.org/10.5194/essd-2025-204
Preprint. Discussion started: 23 June 2025

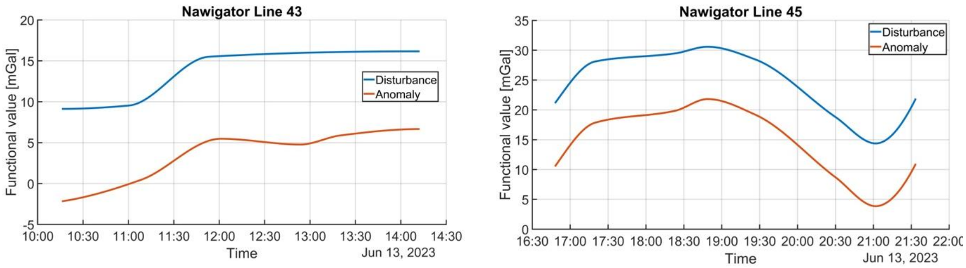

Figure 6: Temporal distribution of gravity anomalies and disturbances on selected measurement profiles conducted by ORP "Heweliusz" (a-d) and s/s "Nawigator XXI" (e-h).

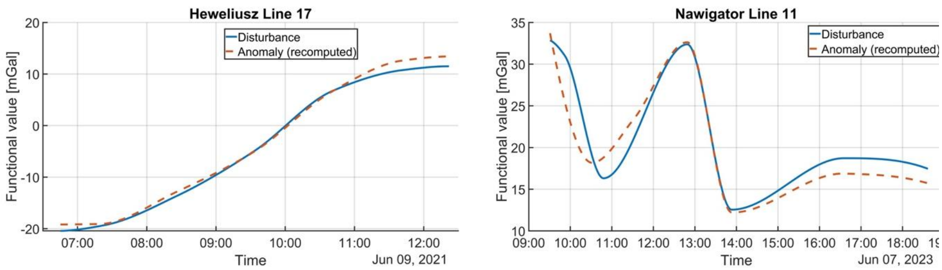

Figure 7: Temporal distribution of shifted gravity anomalies (see below) and disturbances after their reduction on a selected measurement profile conducted by ORP "Heweliusz" and s/s "Nawigator XXI."

From equation (1.11) the offset for different survey lines between the interpreted free-air gravity anomalies and gravity disturbances depends on the height of the geoid surface along the profiles. Processing for both data types was done independently of one another. In order to illustrate to what degree the noisy (standard) corrected measurements, $\tilde{r}_P$, and the processed ellipsoidal heights, h_P, affect the line interpretation, two profiles are shown in Fig. 7, one from each survey. From equation (1.11) the independently processed free-air gravity anomalies were shifted yielding $\Delta g_P - \frac{\partial \gamma}{\partial h} N_P$, where N_P along line profiles are obtained from the EGG2015 model. In this way the individually processed gravity disturbances and gravity anomalies are shown on figures at the same level showing the differences in interpretation.

From equation (1.12), figure 8 shows an example of using both interpreted data types Δg_P and δg_P along a chosen survey line to yield geoidal heights. This is particularly interesting as it allows the geoid surface along the survey lines to be estimated almost directly from marine gravity measurements rather than obtained by surface integration. Figure 8 indicates that it works because the geoid height changes for the chosen profile are reproduced quite well. A different way of looking at this figure is to observe that the difference between the blue and red lines are partly caused by the joint interpretation error by the two methods. The differences, especially big ones, can possibly be traced back to additional corrections on $\tilde{r}_P$ and h_P.

https://doi.org/10.5194/essd-2025-204
Preprint. Discussion started: 23 June 2025

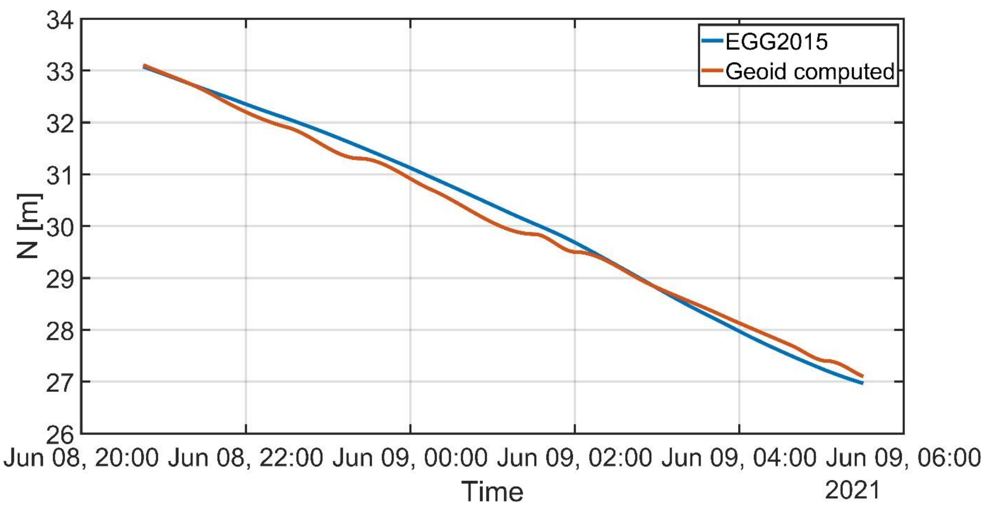

Figure 8: The comparison of the geoid undulation calculated along measurement line no. 15 of ORP Heweliusz campaign and the EGG2015 geoid model. The data is presented in the time domain.

4. DATA AVAILABILITY

The marine gravity dataset used during the analysis presented in the manuscript is available at the online platform Bridge of Data Project under the link https://doi.org/10.34808/30k6-fj34 (Pyrchla Krzysztof et al., 2025) as a single zip archive. The gravity data is stored in csv format, in files Nawigator_XXI_rawgarvity.csv (data collected during s/s "Nawigator XXI" campaign) and ORP_Heweliusz_rawgarvity.csv (data collected during ORP "Heweliusz" campaign). Each file contains table in which each row describes single measurement point, data in columns is as follows:

Year, Month, Day Of Month, Hour, Minute, Second, Milliseconds, RawGravity(mGals), CorrGravity(mGals), FilterWindow(s), FiltCorrGravity(mGals), Long Level(Gals), Cross Level(Gals), Meter temperature(°C), Meter Presures(mbar), Beam(V), VCC effect, Eötvös correction(mGals), IGF correction(mGals), Latitude(deg), Longitude(deg), Course(deg), Speed(kn), MeterStatus, Timer(ms). The data is stored as generated by MGS-6 system. The measurement time is set to UTC.

Gravity data were registered in 2021 and 2023 by a research team from Gdańsk University of Technology during two gravimetric measurement campaigns in the southern Baltic Sea. The campaigns were carried out aboard the Polish Navy research vessel ORP "Heweliusz" and the training ship s/s "Nawigator XXI." The routes were planned according to the needs of gravimetric measurements. In both cases, the MGS-6 Marine Gravity System by Micro-g LaCoste was used. The campaign on ORP "Heweliusz" began on June 6, 2021, at 19:59 in Gdynia Port and ended on June 10, 2021, at 10:53 in the same port. It lasted continuously for 86 hours and 54 minutes. The ship remained in constant motion, as reflected in the GNSS antenna positions.

The campaign on s/s "Nawigator XXI" began on June 5, 2023, at 20:00 in Szczecin Port and ended on June 15, 2023, at 11:30 in the same port. During the voyage, the ship docked in the ports of Rønne (entry on June 6, 2023, at 09:00; departure on June 9, 2023, at 20:00) and Klaipeda (entry on June 10, 2023, at 09:00; departure on June 14, 2023, at 18:00). At both ports, gravimetric points located on the docks were referenced, transferring gravity values from the geodetic control points in Denmark (Bornholm) and Lithuania (Klaipeda).

Position of the vessels was traced using an additional GNSS receiver installed on board. These devices provided data to determine corrections for vertical accelerations caused by the ship's motion and the dynamic effect resulting from the cross-coupling of horizontal and vertical acceleration components. The raw data from these measurements is stored in RINEX 2.11 files. Data from s/s "Nawigator XXI" is stored in NAWIGATORXXI_RINEX subfolder of main zip archive and ORP "Heweliusz" in HEWELIUSZ_RINEX subfolder. The measurement time is set to UTC.

5. CONCLUSION

The question of whether to use gravity anomalies or gravity disturbances in the analysis of marine gravimetric data is academic, at first glance. According to the fundamental equation of relative gravimetry, the nongravitational effects have a direct impact on the absolute gravity values modelled along the measurement profile. Because an absolute gravity value is utilised both in the anomalies and disturbances computations, these effects influence both quantities similarly.

In the gravity disturbance approach, the crucial issue is to ensure that the sensor height measurement error at sea is not significant over any part of the route. We recommend modelling both types of gravity anomalies, because their combination yields a geoid model along the survey line. The geoid model obtained can serve either as a direct estimate of the marine geoid, or, in comparison with existing good quality geoid models for the area, as a means to detect errors in the interpretation of marine gravity readings. This approach is effective since geoid models provide uniform coverage of the Earth's surface, and their accuracy is better than one decimetre in many areas. This allows for straightforward detection of the offset and shape errors in gravity measurements data as well as in GNSS data.

On the other hand, the application of the method for direct geoid estimation leads to the significant increase in the geoid resolution, which is crucial for the modern navigation systems of autonomous vehicles.

We also show that large misfits of the results in cross points between survey lines, after standard corrections, are caused by unmodelled errors included in marine gravimeter readings, such as those caused by weather and sea-state condition and/or to the operational state of the instrument, rather than the gravity signal itself. When these effects are not correctly removed from the marine gravimeter readings, they affect interpretation of the gravity signal along the survey line.

Good statistics at crossover points between survey lines, both internally within a given survey and externally for different surveys, is a consequence of correct modelling of the corrections of marine gravimeter readings in addition to standard corrections.

Author contribution

KP: Methodology, Investigation, Visualization, Writing - Original Draft. GS: Conceptualization, Methodology, Writing - Original Draft. KŁ: Resources, Writing - Original Draft. JK: Supervision, Writing - Review and Editing. JP: Conceptualization, Writing - Original Draft

ACKNOWLEDGMENTS:

The measurement campaigns were co-financed under the projects European Union from the European Regional Development Fund under the 2014-2020:

Operational Programme Smart Growth, the project entitled „Development of technology for acquisition and exploration of gravimetric data of foreshore and seashore of Polish maritime areas" was implemented as part of the National Centre for Research and Development competition: 1/4.1.4/2018 „Application projects"

Interreg Baltic Sea Region 2021-2027. „BalMarGrav -Homogenized marine gravity maps of southern and eastern Baltic Sea for modern 3D applications in marine geodesy, geology and navigation".

Computations were carried out using the computers of Centre of Informatics Tricity Academic Supercomputer & Network

References

Belloni, V., Fugazza, D., and Di Rita, M.: UAV-based glacier monitoring: GNSS kinematic track post-processing and direct georeferencing for accurate reconstructions in challenging environments, The International Archives of the Photogrammetry, Remote Sensing and Spatial Information Sciences, XLIII-B1-2022, 367–373, https://doi.org/10.5194/isprs-archives-XLIII-B1-2022-367-2022, 2022.

Dehlinger, P.: Marine gravity, Elsevier, 1978.

Fors, K., Stenberg, N., and Nilsson, T.: Using the Swedish CORS Network SWEPOS for GNSS Interference Detection, 4323–4333, https://doi.org/10.33012/2021.18113, 2021.

Forsbergbi, R., Olesen, A. V., Alshamsi, A., Gidskehaug, A., Ses, S., Kadir, M., and Peter, B.: Airborne Gravimetry Survey for the Marine Area of the United Arab Emirates, Marine Geodesy, 35, 221–232, https://doi.org/10.1080/01490419.2012.672874, 2012.

Förste, C., Ince, E. S., Johann, F., Schwabe, J., and Liebsch, G.: Marine gravimetry activities on the Baltic Sea in the framework of the EU Project FAMOS, ZfV: Zeitschrift für Geodäsie, Geoinformation und Landmanagement, 145, 287–294, 2020.

https://doi.org/10.5194/essd-2025-204
Preprint. Discussion started: 23 June 2025

Guo, J., Liu, X., Chen, Y., Wang, J., and Li, C.: Local normal height connection across sea with ship-borne gravimetry and GNSS techniques, Marine Geophysical Research, 35, 141–148, https://doi.org/10.1007/s11001-014-9216-x, 2014.

Hofmann-Wellenhof, B. and Moritz, H.: Physical geodesy, Springer Science & Business Media, 2006.

Ince, E. S., Förste, C., Barthelmes, F., Pflug, H., Li, M., Kaminskis, J., Neumayer, K.-H., and Michalak, G.: Gravity Measurements along Commercial Ferry Lines in the Baltic Sea and Their Use for Geodetic Purposes, Marine Geodesy, 43, 573–602, https://doi.org/10.1080/01490419.2020.1771486, 2020.

Johannes, W. J. and Smilde, P. L.: Gravity Anomalies and Disturbances: Reductions and Analyses, in: Gravity Interpretation, Springer Berlin Heidelberg, Berlin, Heidelberg, 151–179, https://doi.org/10.1007/978-3-540-85329-9_4, 2009.

Jonsson, B., Hedling, G., and Wiklund, P.: SWEPOSTM Network-RTK Services-status, applications and experiences, in: Proceedings of the 16th International Technical Meeting of the Satellite Division of The Institute of Navigation (ION GPS/GNSS 2003), 1370–1380, 2003.

Kalaycı, İ., Yüksel, B., and Öğütcü, S.: Impact of Baseline Distance and Interstation Height Difference On the Accuracy of GPS-Derived Station Coordinates, IOP Conf Ser Earth Environ Sci, 44, 042026, https://doi.org/10.1088/1755-1315/44/4/042026, 2016.

Kim, S.-H. and Park, K.-D.: Improving DGPS Accuracy by Considering the Correlation of Pseudorange Correction and Satellite Elevation Angle, Journal of Navigation, 70, 1267–1275, https://doi.org/10.1017/S0373463317000297, 2017.

Kirby, J. F.: On the combination of gravity anomalies and gravity disturbances for geoid determination in Western Australia, J Geod, 77, 433–439, https://doi.org/10.1007/s00190-003-0334-5, 2003.

Koivula, H., Kuokkanen, J., Marila, S., Lahtinen, S., and Mattila, T.: Assessment of sparse GNSS network for network RTK, Journal of Geodetic Science, 8, 136–144, https://doi.org/10.1515/jogs-2018-0014, 2018.

Lidberg, M., Jarlemark, P., Ohlsson, K., and Johansson, J.: Station calibration of the SWEPOS GNSS network, in: FIG, Working Week, 2–6, 2016.

Lu, B., Barthelmes, F., Li, M., Förste, C., Ince, E. S., Petrovic, S., Flechtner, F., Schwabe, J., Luo, Z., Zhong, B., and He, K.: Shipborne gravimetry in the Baltic Sea: data processing strategies, crucial findings and preliminary geoid determination tests, J Geod, 93, 1059–1071, https://doi.org/10.1007/s00190-018-01225-7, 2019.

Panet, I., Kuroishi, Y., and Holschneider, M.: Wavelet modelling of the gravity field by domain decomposition methods: an example over Japan, Geophys J Int, 184, 203–219, https://doi.org/10.1111/j.1365-246X.2010.04840.x, 2011.

Peshekhonov, V. G., Sokolov, A. V., Zheleznyak, L. K., Bereza, A. D., and Krasnov, A. A.: Role of Navigation Technologies in Mobile Gravimeters Development, Gyroscopy and Navigation, 11, 2–12, https://doi.org/10.1134/S2075108720010101, 2020.

Peshekhonov, V. G., Stepanov, O. A., and others: Methods and Technologies for Measuring the Earth's Gravity Field Parameters, Springer, 2022.

Przyborski, M., Pyrchla, J., Pyrchla, K., and Szulwic, J.: MicroGal Gravity Measurements with MGS-6 Micro-g LaCoste Gravimeter, Sensors, 19, 2592, https://doi.org/10.3390/s19112592, 2019.

Pyrchla Krzysztof, Łapiński Kamil, and Pyrchla Jerzy: Marine gravity data of the Southern Baltic Sea region [data set], 2025.

Di Rita, M. and Hanson, K.: Data fusion for construction monitoring: How Leica Infinity manages images, GNSS data, terrestrial scans and BIM data to efficiently track complex construction sites, The International Archives of the Photogrammetry, Remote Sensing and Spatial Information Sciences, XLIII-B2-2022, 373–378, https://doi.org/10.5194/isprs-archives-XLIII-B2-2022-373-2022, 2022.

Sabri, L. M., Sunantyo, T. A., Heliani, L. S., and Widjajanti, N.: Combination of Gravity Disturbances and Gravity Anomalies for Geoid Determination: A Case Study in Semarang City, Central Java, Indonesia, in: 2018 4th International Conference on Science and Technology (ICST), 1–6, https://doi.org/10.1109/ICSTC.2018.8528646, 2018.

Stepanov, O. A., Koshaev, D. A., Motorin, A. V., Krasnov, A. A., and Sokolov, A. V.: Algorithms for Integrated Processing of Marine Gravimeter Data and GNSS Measurements, IFAC-PapersOnLine, 53, 500–505, https://doi.org/10.1016/j.ifacol.2020.12.268, 2020.

Strasser, S., Mayer-Gürr, T., and Zehentner, N.: Processing of GNSS constellations and ground station networks using the raw observation approach, J Geod, 93, 1045–1057, https://doi.org/10.1007/s00190-018-1223-2, 2019.

Tran, D. T., Nguyen, D. H., Luong, N. D., and Dao, D. T.: Impact of the precise ephemeris on accuracy of GNSS baseline in relative positioning technique, VIETNAM JOURNAL OF EARTH SCIENCES, 43, 96–110, https://doi.org/10.15625/0866-7187/15745, 2020.

Appendix A. The two modelling methods explained

In this appendix we explain in some detail the two data processing methods used in this paper. In our mathematical derivations we use standard approximations from a textbook on physical geodesy (Hofmann-Wellenhof and Moritz, 2006). In section A.1 we shortly comment on the fundamental equation of marine gravimetry. The focus is on distinguishing between the "theory" and "practicalities" as experienced by practitioners. The fundamental equation of marine gravimetry is common to both methods. In section A.2, we shortly explain the modelling method of gravity disturbances. This method, which we call a 3D-modelling method, involves detailed modelling/monitoring of the vertical level of the marine gravimeter sensor using the fixed antenna offset on the vessel and 3D GNSS navigation data. We associate this modelling method with highly controlled dedicated marine gravity surveys. In section A.3 we explain the second method of gravity anomaly modelling, which was originally developed for data processing from uncontrolled opportunity marine gravity surveys in Danish waters. We call this method a 2D modelling method because the exact monitoring of the sensor height during the survey was not possible. We find it interesting that a method which was used for processing automated surveys with patchy and incomplete data yields useful results. The same method can also be used to process data collected by dedicated surveys with complete data coverage. In section A.4 we show a surprising consequence if both methods are used on the same data resulting in a marine geoid along the survey lines.

A.1 Fundamental equation of marine gravimetry

A marine gravimeter is a relative gravimeter which adheres to the fundamental equation of relative gravimetry

$$g_P = g_{ref} + \alpha\left[\tilde{r}_P - r_{ref}\right] \qquad \text{(A.1.1)}$$

where g_P is the absolute gravity of a marine gravimeter sensor point P along the survey line, g_{ref} is the reference absolute gravity value in the reference harbor, α is the scale factor of the marine gravimeter, r_{ref} is the (constant) marine gravimeter reading in the reference harbor, and $\tilde{r}_P$ is the corrected marine gravimeter reading associated with the sensor point P.

A few remarks concerning Eq A.1.1:

(a) A marine gravimeter is designed by manufacturers to fulfill Eq A.1.1 in field conditions after standard factory filtering of the raw gravimeter data, and after applying standard corrections described in the instrument's user manual.

(b) It is a common experience among practitioners that despite best efforts, in field conditions the instrument does not always behave as claimed in the manual. Certain external factors associated with turbulent environments at sea (e.g. the sea state and weather) and/or the possibly imperfect operational state of the gravimeter (e.g. the warm-up effect) are difficult to correct for so that the above fundamental equation is calculated accurately.

(c) The apparent requirement of the fundamental equation is a consistent set of defining parameters $\left(g_{ref},\ r_{ref},\ \alpha\right)$ such that the corrected marine gravimeter readings can be translated to gravity differences with respect to g_{ref}. During the reference harbor stay the marine gravimeter is at a specific point in space with respect to the pier. Consistency of the defining parameters implies a reduction of the gravity value measured by the land gravimeters (harbor tie) on a pier in the vicinity of the vessel location, g_{pier}. The reduced gravity value approximates g_{ref} in the fundamental equation of relative gravimetry referring either to the sea-level or to the sensor-level. Without further discussion, the idea of the gravity reduction is to obtain consistency between g_{ref} and r_{ref} to reconcile the true physical conditions (including the gravitational attraction of the pier) during the reference harbor stay. From section A.2, the method of gravity disturbance modelling makes use of reduction to sensor-level after detailed spirit levelling in the reference harbor. The method of free-air gravity modelling described in section A.3 leaves the vertical level at the pier level $g_{ref} = g_{pier}$. Referring to the above principle of consistency of the defining parameters, the consequence of the lack of consistency for g_{ref} is a bias of the results.

(d) The results of marine processing are given along survey lines at sea, i.e. away from the reference harbor. The main processing challenge is to separate in the marine gravity readings the part associated with the gravity signal along the survey lines from the unmodelled misreadings at sea. In simple words, and as discussed in (b), the standard corrections applied to gravity readings are not always sufficient and complete. Additional corrections must be applied. The magnitude of these additional corrections can sometime be much bigger than the gravity reduction from the pier level to the sensor-level, the bias of the results. This justifies why the pier level can be used for absolute gravity reference

$g_{ref} = g_{pier}$.

A.2 The gravity disturbance method

From 3D GNSS navigation data we obtain the ellipsoidal height of the antenna and, via the antenna offset, we get h_P the ellipsoidal height of the sensor at sea. From this we can model the gravity disturbance δg_P (Hofmann-Wellenhof and Moritz, 2006)

$$\delta g_P = g_P - \gamma_{Q=P} \qquad \text{(A.2.1)}$$

at sea.

In order to obtain $\gamma_{Q=P}$ we use a standard approximation (Hofmann-Wellenhof and Moritz, 2006) where we compute γ_{Q_0} on the GRS80 ellipsoid (see Fig. 3.) and use a standard constant free-air normal gravity gradient $\frac{\partial \gamma}{\partial h} = -0.3086$ mGal/m yielding

https://doi.org/10.5194/essd-2025-204
Preprint. Discussion started: 23 June 2025

Open Access Earth System Science Data Discussions

$$\gamma_{Q=P} = \gamma_{Q_0} + \frac{\partial \gamma}{\partial h} h_P \tag{A.2.2}$$

Combining Eq. (A.2.1) with Eq. (A.1.1), the fundamental equation of marine gravimetry, we get

$$\delta g_P = \left[g_{ref} + \alpha \left(\tilde{r}_P - r_{ref} \right) \right] - \left(\gamma_{Q_0} + \frac{\partial \gamma}{\partial h} h_P \right) \tag{A.2.3}$$

Denoting for the reference harbor the gravimeter sensor point P_{ref}, using Eq. (A.2.1) to define $\delta g_{ref} \equiv \delta g_{P_{ref}} = g_{P_{ref}} - \gamma_{Q=P_{ref}}$ and adding on the RHS of Eq. (A.2.3) $\gamma_{Q=P_{ref}} - \gamma_{Q=P_{ref}}$ we arrive after some simple equation algebra to

$$\delta g_P = \left[\delta g_{ref} + \alpha \left(\tilde{r}_P - r_{ref} \right) \right] - \left(\left[\gamma_{Q_0} - \gamma_{Q_{0,ref}} \right] + \frac{\partial \gamma}{\partial h} \left[h_P - h_{P_{ref}} \right] \right) \tag{A.2.4}$$

where $Q_{0,ref}$ is a point on ellipsoid along the ellipsoidal normal through P_{ref}.

A.3 The gravity anomaly method

For the gravity anomaly method we assume that the pier point associated with harbor tie measured in the reference harbor with land gravimeters, P_{pier}, is the reference point P_{ref} associated with the reference absolute gravity value g_{ref} in Eq. (A.1.1). With this definition, there seems to be an apparent mismatch between g_{ref} and r_{ref} in the reference harbor in a sense that these values refer to two different points in space and are, thus, affected differently by the gravitational attraction of the pier. To our knowledge, many practitioners of marine gravimetry put a lot of effort into reducing g_{pier} to either the marine gravimeter sensor height, $g_{ref} = g_{sensor}$, or to the local sea-level $g_{ref} = g_{sea-level}$. This is done by gravity reduction techniques such as free-air gravity reductions and by removing and restoring the gravitational effect of a half Bouguer plate to account consistently for the pier attraction. In fact, in the highly controlled gravity disturbance method that we discuss above this is exactly what is done to obtain $g_{ref} = g_{sensor}$. Nevertheless, the experience from uncontrolled automatic surveys shows that the level of noise on g_P at sea is so high that the careful matching between g_{ref} and r_{ref} in the reference harbor gets lost because certain corrections for e.g. the sea state, the wind and the weather, cannot be done so accurate so that the matching between g_P and $\tilde{r}_P$ while at sea is maintained.

Keeping the definition of g_{ref} as described above the advantage is geodetic control from land. The pier point can be visited with portable RTK antenna so that the orthometric height of the pier point in the national height system H_{pier} and the ellipsoidal height h_{pier} can be measured to high accuracy. From this we can determine the free-air gravity anomaly for the pier point Δg_{pier}:

https://doi.org/10.5194/essd-2025-204
Preprint. Discussion started: 23 June 2025

$$\Delta g_{pier} = g_{pier} - \left[\gamma_{0,pier} + \frac{\partial \gamma}{\partial h} H_{pier} \right] \tag{A.3.1}$$

where $\gamma_{0,pier}$ is the normal gravity on ellipsoid for the pier point.

Let us define a virtual point at sea P^* in the same orthometric height above the geoid H_{P^*} as the pier point in the reference harbor, $H_{P^*} = H_{pier}$. We can compute free-air gravity anomaly for such virtual point at sea as

$$\Delta g_{P^*} = g_{P^*} - \left[\gamma_{0,P^*} + \frac{\partial \gamma}{\partial h} H_{P^*} \right] \tag{A.3.2}$$

Using Eq. (A.1.1) for the virtual point, i.e. $P = P^*$, we get

$$g_{P^*} = g_{pier} + \alpha \left[\tilde{r}_{P^*} - r_{ref} \right] \tag{A.3.3}$$

which can be “expanded” to the following lengthy expression

$$g_{P^*} - \left[\gamma_{0,P^*} + \frac{\partial \gamma}{\partial h} H_{P^*} \right] = g_{pier} + \alpha \left[\tilde{r}_{P^*} - r_{ref} \right] - \left[\gamma_{0,P^*} + \frac{\partial \gamma}{\partial h} H_{P^*} \right] \tag{A.3.4}$$

which by adding on the RHS of the equation $\left[\gamma_{0,pier} + \frac{\partial \gamma}{\partial h} H_{pier} \right] - \left[\gamma_{0,pier} + \frac{\partial \gamma}{\partial h} H_{pier} \right] = 0$ and after some elementary algebra and using Eq. (A.3.1) and Eq. (A.3.2) we get:

$$\Delta g_{P^*} = \Delta g_{pier} + \alpha \left[\tilde{r}_{P^*} - r_{ref} \right] - \left[\gamma_{0,P^*} + \frac{\partial \gamma}{\partial h} H_{P^*} \right] + \left[\gamma_{0,pier} + \frac{\partial \gamma}{\partial h} H_{pier} \right] \tag{A.3.5}$$

Finally, using $H_{P^*} = H_{pier}$ we get

$$\Delta g_{P^*} = \Delta g_{pier} + \alpha \left[\tilde{r}_{P^*} - r_{ref} \right] + \left[\gamma_{0,pier} - \gamma_{0,P^*} \right] \tag{A.3.6}$$

which corresponds to Eq. (A,1.1) but for the free-air gravity anomalies instead of absolute gravity.

The advantage of the above equation is that free-air gravity anomalies are only weakly dependent on height. Starting with the definition of free-air gravity anomalies for the marine gravity sensor point P where the orthometric height of this point H_P is unknown for this method we have:

$$\Delta g_P = g_P - \left[\gamma_{Q_0} + \frac{\partial \gamma}{\partial h} H_P \right] = \left[g_{P_0} + \frac{\partial g}{\partial h} H_P \right] - \left[\gamma_{Q_0} + \frac{\partial \gamma}{\partial h} H_P \right] \tag{A.3.7}$$

Leading to

$$\Delta g_P = \left[g_{P_0} + \frac{\partial g}{\partial h} H_{P^*} \right] - \left[\gamma_{Q_0} + \frac{\partial \gamma}{\partial h} H_{P^*} \right] + \left[\left(\frac{\partial g}{\partial h} - \frac{\partial \gamma}{\partial h} \right) \left(H_P - H_{P^*} \right) \right] \tag{A.3.8}$$

Yielding

$$\Delta g_P = \Delta g_{P^*} + \left(\frac{\partial g}{\partial h} - \frac{\partial \gamma}{\partial h} \right) \left(H_P - H_{P^*} \right) \tag{A.3.9}$$

https://doi.org/10.5194/essd-2025-204
Preprint. Discussion started: 23 June 2025

Using following approximation $\frac{\partial g}{\partial h} \approx \frac{\partial \gamma}{\partial h} = -0.3086$ mGal/m, we get

$$\Delta g_P \approx \Delta g_{P^*} \tag{A.3.10}$$

A.4 Geoidal height N_P from Δg_P and δg_P

Using Helmert's projection (Hofmann-Wellenhof and Moritz, 2006) , where the orthometric height is projected on the ellipsoidal normal, $h_P = H_P + N_P$ for the sensor point P and using a corresponding equation to Eq. (A.3.4), but for gravity disturbances

$$\delta g_P = g_P - \left[\gamma_{Q_0} + \frac{\partial \gamma}{\partial h} h_P\right] = g_P - \left[\gamma_{Q_0} + \frac{\partial \gamma}{\partial h}\left(H_P + N_P\right)\right] \tag{A.4.1}$$

we finally obtain

$$\delta g_P = \Delta g_P - \frac{\partial \gamma}{\partial h} N_P \tag{A.4.2}$$

Yielding

$$N_P = \left(\Delta g_P - \delta g_P\right) / \left(\partial \gamma / \partial h\right) \tag{A.4.3}$$

This derivation is consistent with formulas presented in (Kirby, 2003)